Preprint Title Synthesis and Photophysical and Electrochemical Properties of Pyridine-, Pyrazine- and Triazine-based (D-π-)$_2$A Fluorescent Dyes

Authors Keiichi Imato, Toshiaki Enoki, Koji Uenaka and Yousuke Ooyama

Article Type Full Research Paper

Supporting Information File 1 Supporting Information-Ooyama et al.doc; 449.5 KB

ORCID® iDs Yousuke Ooyama - https://orcid.org/0000-0002-0257-6930

Synthesis and Photophysical and Electrochemical Properties of Pyridine-, Pyrazine- and Triazine-based (D-π-)$_2$A Fluorescent Dyes

Keiichi Imato, Toshiaki Enoki, Koji Uenaka and Yousuke Ooyama*

Address: Department of Applied Chemistry, Graduate School of Engineering, Hiroshima University, 1-4-1 Kagamiyama, Higashi-Hiroshima 739-8527, Japan.

Email: Yousuke Ooyama* - yooyama@hiroshima-u.ac.jp

* Corresponding author

Abstract

Donor–acceptor–π-conjugated (D–π–)$_2$A fluorescent dyes **OUY-2**, **OUK-2** and **OUJ-2** with two (diphenylamino)carbazole-thiophene units as D (electron-donating group)–π (π-conjugated bridge) moiety and a pyridine, pyrazine or triazine ring as electron-withdrawing group (electron-accepting group; A) have been designed and developed and their photophysical and electrochemical properties were investigated based on the photoabsorption and fluorescence spectroscopy, Lippert–Mataga plots, cyclic voltammetry and density functional theory calculations. The photoabsorption maximum (λ^{abs}_{max}) and the fluorescence maximum (λ^{fl}_{max}) for the intramolecular charge-transfer characteristic band of the (D–π–)$_2$A fluorescent dyes show bathochromic shift in the order of **OUY-2** < **OUK-2** < **OUJ-2**. Moreover, the photoabsorption spectra of the (D–π–)$_2$A fluorescent dyes are nearly independent of solvent polarity, while their fluorescence maxima bathochromically shifted with

increasing solvent polarity (*i.e.*, positive fluorescence solvatochromism). The Lippert–Mataga plots for **OUY-2**, **OUK-2** and **OUJ-2** indicate that the $\Delta\mu$ (= $\mu_e - \mu_g$) value, which is the difference in the dipole moment of the dye between the excited (μ_e) and the ground (μ_g) states, increases in the order of **OUY-2** < **OUK-2** < **OUJ-2**, that is, the fact explains our findings that **OUJ-2** shows large bathochromic shifts in their fluorescence maxima in polar solvents and that the Stokes shift values for **OUJ-2** in polar solvents are much larger than those in nonpolar solvents. The cyclic voltammetry of **OUY-2**, **OUK-2** and **OUJ-2** demonstrated that there is little difference in the HOMO energy level among the three dyes, but the LUMO energy levels decrease in the order of **OUY-2** > **OUK-2** > **OUJ-2**. Consequently, this work reveals that for the $(D–\pi–)_2A$ fluorescent dyes **OUY-2**, **OUK-2** and **OUJ-2** the bathochromic shifts of λ^{abs}_{max} and λ^{fl}_{max} and the lowering of the LUMO energy level are dependent on the electron-withdrawing ability of azine ring, which increases in the order of **OUY-2** < **OUK-2** < **OUJ-2**.

Keywords

fluorescent dyes; pyridine; pyrazine; triazine; D-π-A structure

Introduction

Donor–acceptor–π-conjugated (D–π–A) dyes, which are constructed of the electron-donating group (D) such as a diphenyl- or dialkylamino group and the electron-withdrawing group (electron-accepting group; A) such as a nitro, cyano, and carboxyl group and a azine ring such as pyrizine, pyrazine and triazine linked by the π-conjugated bridges such as oligoene and heterocycles, exhibit intense photoabsorption and fluorescence emission properties based on the intramolecular

charge transfer (ICT) excitation from the D moiety to the A moiety [1-4]. D–π–A structure possess a considerable structural characteristics that the increase in the electron-donating and electron-accepting abilities of D and A moieties and the expansion of π conjugation, respectively, can lead to the decrease in the energy gap between the HOMO and LUMO because the highest occupied molecular orbital (HOMO) is localized over the π-conjugated system containing the D moiety, and the lowest unoccupied molecular orbital (LUMO) is localized over the A moiety. Thus, the photophysical and electrochemical properties based on the ICT characteristics of D–π–A dyes should be tunable by not only the electron-donating ability of D and the electron-accepting ability of A, but also the electronic characteristics of the π bridge. Consequently, D–π–A dyes are of considerable practical concern as useful fluorescence sensors for cation, anion and neural species [5-14], efficient emitters for organic light emitting diodes (OLEDs) [15-24], and promising photosensitizers for dye-sensitized solar cells (DSSCs) [25-34].

Thus, in this work, to gain insight into photophysical and electrochemical properties of D–π–A fluorescent dyes with azine ring as electron-withdrawing group, we have designed and synthesized $(D–π–)_2A$ fluorescent dyes **OUY-2**, **OUK-2** and **OUJ-2** with two (diphenylamino)carbazole-thiophene units as D–π moiety and a pyridine, pyrazine or triazine ring as A moiety (Figure 1). An advantage of $(D–π–)_2A$ fluorescent dyes over other D–π–A fluorescent dyes is the broad and intense photoabsorption spectral features. Herein, based on the photoabsorption and fluorescence spectroscopy, Lippert–Mataga plots, cyclic voltammetry and density functional theory (DFT) calculations, we reveal the photophysical and electrochemical properties of the $(D–π–)_2A$ fluorescent dyes **OUY-2**, **OUK-2** and **OUJ-2**.

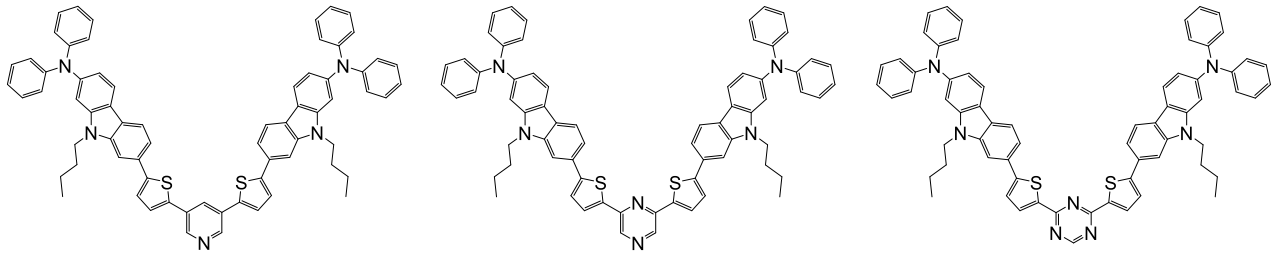

OUY-2 **OUK-2** **OUJ-2**

Figure 1: Chemical structures of (D–π–)$_2$A fluorescent dyes **OUY-2**, **OUK-2** and **OUJ-2**.

Results and Discussion

Synthesis

The (D–π–)$_2$A fluorescent dyes **OUY-2** [2], **OUK-2** [3, 4] and **OUJ-2** were prepared by Stille coupling of stannyl compound **1** [3] with 3,5-dibromopyridine, 2,6-diiodopyrazine, and 2,4-dichloro-1,3,5-triazine, respectively (Scheme 1, see Experimental for synthetic procedure of **OUJ-2**).

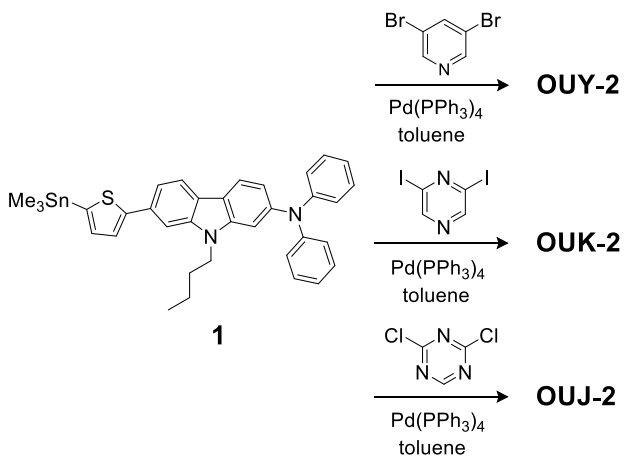

Scheme 1: Synthesis of **OUY-2**, **OUK-2** and **OUJ-2**.

Optical properties

The photoabsorption and fluorescence spectra of **OUY-2**, **OUK-2** and **OUJ-2** in various solvents are shown in Figure 2, and their optical data are summarized in Table 1. The **OUY-2**, **OUK-2** and **OUJ-2** in toluene as a non-polar solvent show the photoabsorption maximum (λ^{abs}_{max}) at 398 nm, 401 nm and 433 nm, respectively, which is assigned to the ICT excitation from the two (diphenylamino)carbazole-thiophene units as D–π moiety to a pyridine, pyrazine or triazine ring as A moiety. For **OUK-2**, the shoulder band was observed at around 430 nm. Thus, the ICT-based photoabsorption band of the three dyes appears at a longer wavelength region in the order of **OUY-2** < **OUK-2** < **OUJ-2**, which is in agreement with increase in the electron-withdrawing ability of azine ring in the order of pyridyl group < pyrazyl group < triazyl group. The photoabsorption spectra of the three dyes are nearly independent of solvent polarity. This indicates that the electronic and structural characteristics of the ground and Franck–Condon (FC) excited states do not differ much with a change in solvent polarity. The molar extinction coefficient (ε_{max}) for the ICT band is ca. 100000 M^{-1} cm^{-1} for **OUY-2**, 75000 M^{-1} cm^{-1} for **OUK-2** and 80000 M^{-1} cm^{-1} for **OUJ-2**. The corresponding fluorescence maximum (λ^{fl}_{max}) of the three dyes in toluene also appears at a longer wavelength region in the order of **OUY-2** (453 nm) < **OUK-2** (480 nm) < **OUJ-2** (509 nm). Interestingly, in contrast to the photoabsorption spectra, the fluorescence spectra are strongly dependent on solvent polarity, that is, the three dyes showed bathochromic shifts of the fluorescence band with increasing solvent polarity from toluene to DMF (*i.e.*, positive fluorescence solvatochromism). Thus, the Stokes shift (SS) values of the three dyes increase with increasing solvent polarity. Compared with **OUY-2**, **OUK-2** and **OUJ-2** exhibit significant fluorescence solvatochromic properties but a significant decrease in the fluorescence quantum yield (Φ_f) in polar solvent such as DMF (Φ_f = 0.59, 0.14 and

0.09 for **OUY-2**, **OUK-2** and **OUJ-2**, respectively), although **OUK-2** and **OUJ-2** exhibit a higher Φ_f value (0.48–0.65 and 0.72–0.86, respectively) in relatively low polar solvents than **OUY-2** (Φ_f = 0.38–0.58).

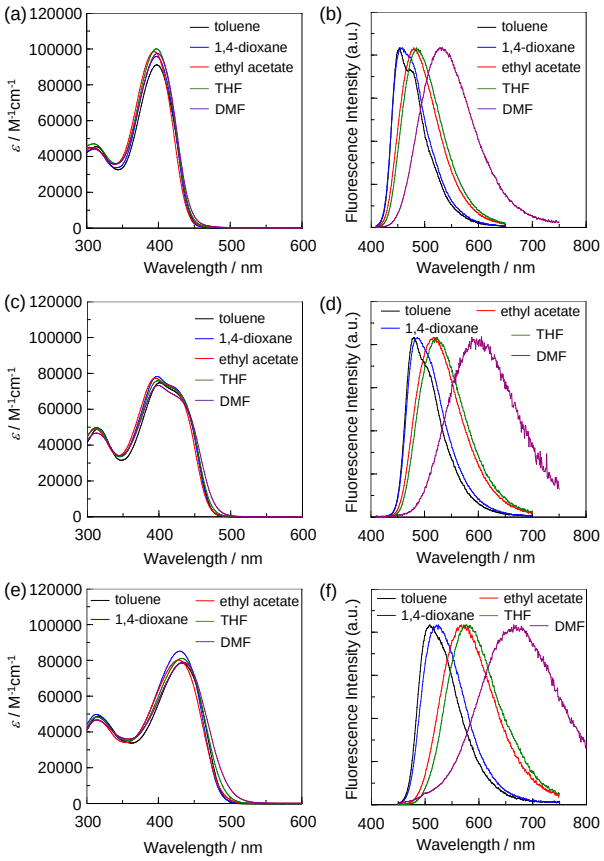

Figure 2: (a) Photoabsorption and (b) fluorescence (λ^{ex} = ca. 400 nm) spectra of **OUY-2** in various solvents. (c) Photoabsorption and (d) fluorescence (λ^{ex} = ca. 400 nm) spectra of **OUK-2** in various solvents. (a) Photoabsorption and (b) fluorescence (λ^{ex} = ca. 430 nm) spectra of **OUJ-2** in various solvents.

Table 1: Optical data of **OUY-2**, **OUK-2** and **OUJ-2** in various solvents.

Dye	Solvent	λ^{abs}_{max} [nm] (ε [$M^{-1}cm^{-1}$])	λ^{fl}_{max} [nm] (Φ_f)[a]	Stokes shift [cm^{-1}]
OUY-2	Toluene	398 (91100)	453 (0.38)	3050
	1,4-Dioxane	398 (995800)	455 (0.40)	3147
	Ethyl acetate	394 (98500)	480 (0.39)	4547
	THF	397 (100000)	485 (0.58)	4570
	DMF	399 (97500)	533 (0.59)	6300
OUK-2	Toluene	401 (74800)	480 (0.48)	4104
	1,4-Dioxane	397 (78300)	487 (0.62)	4655
	Ethyl acetate	398 (75800)	518 (0.55)	5820
	THF	394 (77400)	524 (0.65)	6296
	DMF	399 (73300)	588 (0.14)	8055
OUJ-2	Toluene	433 (78570)	509 (0.81)	3448
	1,4-Dioxane	430 (85100)	525 (0.86)	4208
	Ethyl acetate	428 (80100)	568 (0.72)	5758
	THF	433 (81100)	576 (0.72)	5733
	DMF	435 (78900)	665 (0.09)	7950

[a]Fluorescence quantum yields (Φ_f) were determined by using a calibrated integrating sphere system (λ^{ex} = 400 nm for **OUY-2**, 400 nm for **OUK-2**, and 430 nm for **OUJ-2**, respectively).

It is well accepted that the dipole–dipole interactions between the fluorescent dye and solvent molecules are responsible for the solvent-dependent shifts in the fluorescence maxima [35-43]. Therefore, in order to understand the fluorescence solvatochromisms of **OUY-2**, **OUK-2** and **OUJ-2**, we have investigated the

relationships between the solvent polarity-dependent shift of fluorescence maximum and the dipole moment of the dye molecule on the basis of the Lippert–Mataga equation [eqn (1)]: [44-46]

$$v_{st} = \frac{1}{4\pi\varepsilon_0} \cdot \frac{2\Delta\mu^2}{hca^3} \Delta f + \text{Const.} \qquad (1)$$

where

$$\Delta f = \frac{\varepsilon - 1}{2\varepsilon + 1} - \frac{n^2 - 1}{2n^2 + 1} \qquad (2)$$

Consequently, on the basis of eqns (1) and (2), the change in dipole moment, $\Delta\mu = \mu_e - \mu_g$, between the ground ($\mu_g$) and the excited ($\mu_e$) states can easily be evaluated from the slope of a plot of v_{st} against Δf (the Lippert–Mataga plot), where v_{st} is the Stokes shift (Table 1), ε_0 is the vacuum permittivity, h is Planck's constant, c is the velocity of light, a is the Onsager radius of the dye molecule (7.81 Å, 7.99 Å and 7.91 Å for **OUY-2**, **OUK-2** and **OUJ-2**, respectively, estimated from DFT calculation at the B3LYP/6-31G(d,p) level [47]), Δf is the orientation polarizability, ε is the static dielectronic constant, and n is the refractive index of the solvent. The Lippert–Mataga plots (Figure 3) for the three dyes show high linearity, indicating that for the three dyes the solvent-dependent shift in the fluorescence maximum is mainly attributed to the dipole–dipole interactions between the dye molecule and solvent molecule. The slopes (m_{sl}) became steep in the order of **OUY-2** (10500 cm^{-1}) < **OUK-2** (12200 cm^{-1}) < **OUJ-2** (13700 cm^{-1}). The $\Delta\mu$ values increase in the order of **OUY-2** (22 D) < **OUK-2** (25 D) < **OUJ-2** (26 D), which corresponds to the increase in the electron-withdrawing ability of azine ring (pyridyl group < pyrazyl group < triazyl group). Consequently, the Lippert–Mataga plots explains our findings that **OUJ-2** shows

large bathochromic shifts in its fluorescence maxima in polar solvents and that the Stokes shift values for **OUJ-2** in polar solvents are much larger than those in nonpolar solvents (Table 1).

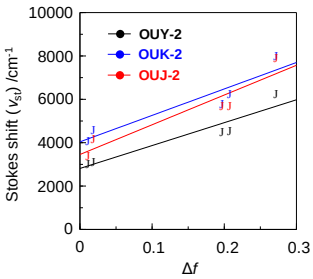

Figure 3: Correlation of the Stokes shift (ν_{st}) and the orientation polarizability (Δf) according to eqn (1) and (2), respectively, for **OUY-2**, **OUK-2** and **OUJ-2**; solvent (ε, n, Δf) : toluene (2.38, 1.4969, 0.0132), 1,4-dioxane (2.21, 1.4224, 0.0205), ethyl acetate (6.02, 1.3724, 0.199), THF (7.58, 1.4072, 0.2096) and DMF (36.71, 1.4305, 0.274) [4].

In order to investigate the solid-state photophysical properties of **OUY-2**, **OUK-2** and **OUJ-2**, we have measured the solid-state fluorescence spectra of the solids (Figure 4). The λ^{fl}_{max} of the as-recrystallized dyes appears at 550 nm for **OUY-2**, 592 nm for **OUK-2**, and 557 nm for **OUJ-2**, which shifted significantly and bathochromically by 97 nm, 112 nm, and 48 nm, respectively, compared with those in toluene. The solid-state Φ_f value is below 0.02 for **OUY-2** and **OUK-2** and 0.09 for **OUJ-2**, which are much lower than those in toluene. It is well known that D-π-A fluorescent dyes show bathochromic shift of λ^{fl}_{max} and the lowering of Φ_f value by changing from the solution state to the solid state, which are attributed to the delocalization of excitons or excimers due to the formation of intermolecular π-π interactions [48-51] between the dye molecules in the solid state, although we could

not prepare single crystals of **OUY-2**, **OUK-2** and **OUJ-2** for the X-ray structural analysis.

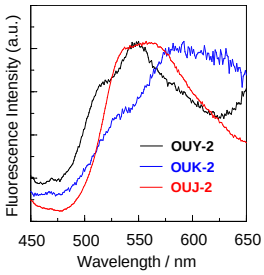

Figure 4: Fluorescence spectra of **OUY-2** (λ^{ex} = 370 nm), **OUK-2** (λ^{ex} = 370 nm) and **OUJ-2** (λ^{ex} = 380 nm) in the solid-state.

Electrochemical properties

The electrochemical properties of **OUY-2**, **OUK-2** and **OUJ-2** were investigated using cyclic voltammetry (CV) in DMF containing 0.1 M tetrabutylammonium perchlorate (Bu_4NClO_4). The cyclic voltammograms of the three dyes are shown in Figure 5. The reversible oxidation waves (E_{pc}^{ox}) for the three dyes were observed at 0.42 V for **OUY-2** and **OUK-2** and 0.45 V for **OUJ-2**, vs. ferrocene/ferrocenium (Fc/Fc^+) (Table 2). The corresponding reduction waves (E_{pa}^{ox}) appeared at 0.35 V for **OUY-2** and **OUK-2** and 0.36 V for **OUJ-2**, thus indicating that the three dyes undergo an electrochemically stable oxidation–reduction process. The HOMO energy level (–[$E_{1/2}^{ox}$ + 4.8] eV) *versus* the vacuum level was estimated from the half-wave potential for oxidation ($E_{1/2}^{ox}$ = 0.39 V for **OUY-2** and **OUK-2** and 0.40 V for **OUJ-2**). Therefore, the HOMO energy level was –5.19 eV for **OUY-2** and **OUK-2** and –5.20 eV for **OUJ-2**, respectively, thus indicating that the three dyes have comparable HOMO energy levels. The LUMO energy level *versus* the vacuum level was evaluated from the

$E_{1/2}^{ox}$ and an intersection of photoabsorption and fluorescence spectra (449 nm; 2.76 eV for **OUY-2**, 481 nm; 2.58 eV for **OUK-2**, 506 nm; 2.45 eV for **OUJ-2**) in DMF, that is, the LUMO energy level was obtained through eqn = [HOMO + E_{0-0}] eV, where E_{0-0} transition energy is the intersection of the photoabsorption and fluorescence spectra corresponding to the optical energy gap between the HOMO and the LUMO. Thus, the LUMO energy level *versus* the vacuum level is lowered in the order of **OUY-2** (–2.43 eV) > **OUK-2** (–2.61 eV) > **OUJ-2** (–2.75 eV), showing that increasing the electron-withdrawing ability of azine ring lowers the LUMO energy level of the $(D–\pi–)_2A$ fluorescent dyes. Consequently, the fact revealed that the bathochromic shift of the ICT-based photoabsorption band in the order of **OUY-2** < **OUK-2** < **OUJ-2** is attributed to stabilization of the LUMO level because of the increase in the electron-withdrawing ability of azine ring in the order of pyridyl group < pyrazyl group < triazyl group, resulting in a decrease in energy gap between the HOMO and LUMO.

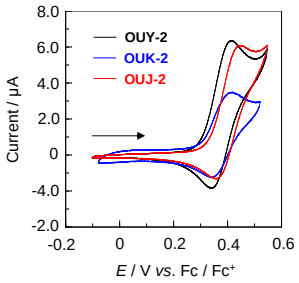

Figure 5: Cyclic voltammograms of **OUY-2**, **OUK-2** and **OUJ-2** in DMF containing 0.1 M Bu_4NClO_4. The arrow denotes the direction of the potential scan.

Table 2: Electrochemical data, and HOMO and LUMO energy level of **OUY-2, OUK-2** and **OUJ-2**.

Dye	E_{pc}^{ox} [V][a]	E_{pa}^{ox} [V][a]	$E_{1/2}^{ox}$ [V][a]	HOMO [eV][b]	LUMO [eV][c]	E_{0-0} [eV][d]
OUY-2	0.42	0.35	0.39	–5.19	–2.43	2.76 eV
OUK-2	0.42	0.35	0.39	–5.19	–2.61	2.58 eV
OUJ-2	0.45	0.36	0.40	–5.20	–2.75	2.45 eV

[a]The anodic peak (E_{pc}^{ox}), the cathodic peak (E_{pc}^{ox}) and the half-wave ($E_{1/2}^{ox}$) potentials for oxidation *vs*. Fc/Fc^+ were recorded in DMF/Bu_4NClO_4 (0.1M) solution; [b]the HOMO energy level (– [$E^{ox}_{1/2}$ + 4.8] eV) *versus* the vacuum level was evaluated from the $E_{1/2}^{ox}$ for oxidation; [c]the LUMO energy level *versus* the vacuum level was evaluated from the HOMO and the optical energy gap (E_{0-0}), that is, the LUMO energy level was obtained through eqn = [HOMO + E_{0-0}] eV; [d]the optical energy gap (E_{0-0}) was determined from the intersection of photoabsorption and fluorescence spectra in DMF.

Theoretical calculations

In order to examine the HOMO and LUMO distributions of **OUY-2**, **OUK-2** and **OUJ-2**, the molecular structures and molecular orbitals of the three dyes were calculated using the DFT at the B3LYP/6-31G(d,p) level [47]. The result of the DFT calculation for the three dyes indicated that the HOMO is mostly localized on the two (diphenylamino)carbazole moieties containing the thiophene ring and the LUMO is mostly localized on the thienylpyridine moiety for **OUY-2**, thienylpyrazine moiety for **OUK-2** and thienyltriazine moiety for **OUJ-2** (Figure 6). Accordingly, the DFT calculations reveal that the photoexcitation of **OUY-2**, **OUK-2** and **OUJ-2** induces the ICT from the two (diphenylamino)carbazole moieties to each azine ring. The HOMO

energy level of the three dyes is remarkably similar to each other (–4.80 eV, –4.78 eV and –4.84 eV for **OUY-2**, **OUK-2** and **OUJ-2**, respectively), and the LUMO energy level is lowered in the order of **OUY-2** (–1.56 eV) > **OUK-2** (–1.76 eV) > **OUJ-2** (–1.98 eV), which are in good agreement with the experimental results from the photoabsorption and fluorescence spectral analyses (Figure 2) and the cyclic voltammetry (Figure 5). Thus, the experimental results and the DFT calculation strongly demonstrated that the bathochromic shift of the ICT-based photoabsorption band in the order of **OUY-2** < **OUK-2** < **OUJ-2** is attributed to stabilization of the LUMO energy level due to the increase in the electron-withdrawing ability of azine ring in the order of pyridyl group < pyrazyl group < triazyl group.

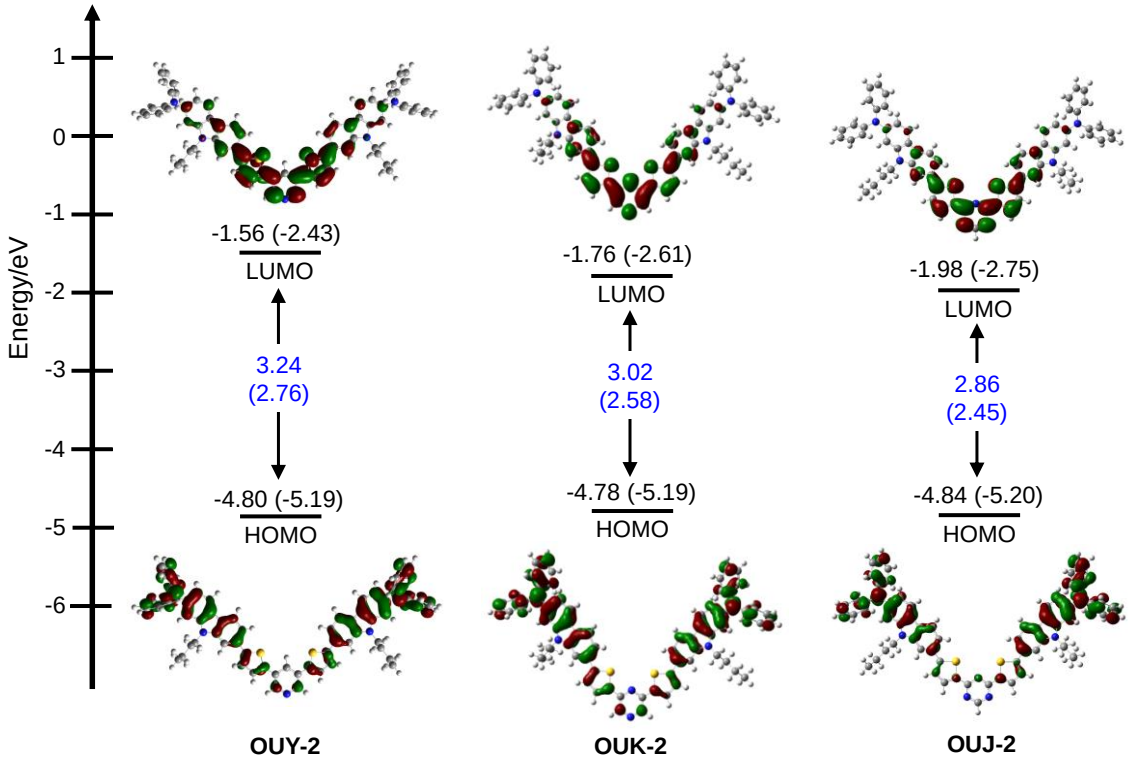

Figure 6: Energy level diagram, HOMO and LUMO of **OUY-2**, **OUK-2** and **OUJ-2**, derived from the DFT calculations at B3LYP/6-31G(d,p) level. Numbers in parentheses are the experimental values.

Conclusion

To gain insight into photophysical and electrochemical properties of D–π–A fluorescent dyes with azine ring as electron-withdrawing group, we have designed and synthesized a new type of $(D–π–)_2A$ fluorescent dyes **OUY-2**, **OUK-2** and **OUJ-2** with two (diphenylamino)carbazole-thiophene units as D (electron-donating group)–π (π-conjugated bridge) moiety and a pyridine, pyrazine or triazine ring as electron-withdrawing group (electron-accepting group; A), and their photophysical and electrochemical properties were investigated. It was found that the intramolecular charge-transfer (ICT)-based photoabsorption and fluorescence bands of the three dyes appear at a longer wavelength region in the order of **OUY-2** < **OUK-2** < **OUJ-2**, which is due to the increase in the electron-withdrawing ability of azine ring in the order of pyridyl group < pyrazyl group < triazyl group. Moreover, the $(D–π–)_2A$ fluorescent dyes showed a large bathochromic shift of fluorescence maxima with increasing solvent polarity (*i.e.*, positive fluorescence solvatochromism). The Lippert–Mataga plots revealed that the difference in the dipole moment of the dye between the excited and the ground states increase in the order of **OUY-2** < **OUK-2** < **OUJ-2**, that is, the fact explains our findings that **OUJ-2** shows large bathochromic shifts in their fluorescence maxima in polar solvents and that the Stokes shift values for **OUJ-2** in polar solvents are much larger than those in nonpolar solvents. The cyclic voltammetry and DFT calculations demonstrated that the HOMO energy level of the three dyes is remarkably similar to each other, but the LUMO energy level is lowered in the order of **OUY-2** > **OUK-2** > **OUJ-2**, showing that increasing the electron-withdrawing ability of azine ring lowers the LUMO energy level of the $(D–π–)_2A$ fluorescent dyes. Consequently, this work reveals that for the $(D–π–)_2A$ fluorescent dyes **OUY-2**, **OUK-2** and **OUJ-2**, the bathochromic shift of photoabsorption and

fluorescence maxima and the lowering of LUMO energy level are dependent on the electron-withdrawing ability of azine ring which increases in the order of **OUY-2** < **OUK-2** < **OUJ-2**.

Experimental

General methods

Melting points were measured with a Yanaco micro melting point apparatus MP model. FT-IR spectra were recorded on a SHIMADZU IRAffinity-1 spectrometer by ATR method. High-resolution mass spectral data were acquired on a Thermo Fisher Scientific LTQ Orbitrap XL. ^{1}H NMR and ^{13}C NMR spectra were recorded on a Varian-400 (400 MHz) FT NMR spectrometer. Photobsorption spectra were observed with a HITACHI U-2910 spectrophotometer, and fluorescence spectra were measured with a HORIBA FluoroMax-4 spectrofluorometer. The fluorescence quantum yields in solution were determined by a HORIBA FluoroMax-4 spectrofluorometer by using a calibrated integrating sphere system. Cyclic voltammetry (CV) curves were recorded in DMF/Bu_4NClO_4 (0.1 M) solution with a three-electrode system consisting of Ag/Ag^+ as reference electrode, Pt plate as working electrode, and Pt wire as counter electrode by using a Electrochemical Measurement System HZ-7000 (HOKUTO DENKO).

Synthesis

General synthetic procedure of (D-π-)$_2$A fluorescent dyes OUY-2, **OUK-2** and **OUJ-2**

OUY-2 [2], **OUK-2** [3] and **OUJ-2** were prepared by Stille coupling of stannyl compound **1** [3] with 3,5-dibromopyridine, 2,6-diiodopyrazine, and 2,4-dichloro-1,3,5-

triazine, respectively, by using $Pd(PPh_3)_4$ as a catalyst in toluene at 110 ºC under an argon atmosphere (Scheme 1).

Synthesis of OYJ-2: A solution of **1** [3] (0.60 g, 0.95 mmol), 2,4-dichloro-1,3,5-triazine (0.071 g, 0.48 mmol), and $Pd(PPh_3)_4$ (0.18 g, 0.16 mmol) in toluene (10 mL) was stirred for 48 h at 110 ºC under an argon atmosphere. After concentrating under reduced pressure, the resulting residue was dissolved in dichloromethane and washed with water. The dichloromethane extract was evaporated under reduced pressure. The residue was chromatographed on silica gel (ethyl acetate : dichloromethane = 1 : 4 as eluent) to give **OUJ-2** (0.38 g, yield 70%) as a yellow solid; m.p. 267–269 °C; IR (ATR): $\tilde{\nu}$ = 1594, 1548, 1491 cm^{-1}; ^1H NMR (400 MHz, CD_2Cl_2) δ = 0.89 (t, J = 7.3 Hz, 6H), 1.29-1.35 (m, 4H), 1.75-1.83 (m, 4H), 4.22 (t, J = 7.1 Hz, 4H), 6.96 (dd, J = 1.8 and 8.4 Hz, 2H), 7.02-7.06 (m, 4H), 7.13-7.16 (m, 10H), 7.26-7.30 (m, 8H), 7.57 (d, J = 4.0 Hz, 2H), 7.60-7.63 (dd, J = 8.1 and 1.5 Hz, 2H), 7.72 (s, 2H), 7.95 (d, J = 8.4 Hz, 2H), 8.04 (d, J = 8.1 Hz, 2H), 8.27 (d, J = 4.0 Hz, 2H), 9.00 (s, 1H) ppm; ^{13}C NMR (100 MHz, CD_2Cl_2) δ = 14.04, 20.86, 31.47, 43.10, 105.17, 106.55, 117.52, 117.92, 118.47, 120.53, 121.40, 123.08, 123.94, 124.50, 124.79, 129.58, 130.62, 133.57, 139.41, 141.56, 142.95, 147.31, 148.55, 153.55, 167.62 ppm (one aromatic carbon signal was not observed owing to overlapping resonances); HRMS (ESI): *m*/*z* (%): $[M+H^+]$ calcd for $C_{67}H_{56}N_7S_2$, 1022.40331, found 1022.40344.

Supporting Information

Supporting Information File 1:

^1H and ^{13}C NMR spectra of **OUJ-2**.

Acknowledgements

This work was supported by a Grant-in-Aid for Scientific Research on Innovative Areas “Soft Crystals” (No. 2903) (JSPS KAKENHI Grant No. 18H04520) and for Scientific Research (B) (JSPS KAKENHI Grant No. 19H02754), and by Shorai Foundation for Science and Technology.

References

1. Ooyama, Y.; Uenaka, K.; Ohshita, J. *RSC Adv*. **2015**, *5*, 21012–21018. doi:10.1039/c4ra16399k

2. Ooyama, Y.; Uenaka, K.; Ohshita, J. *Eur. J. Org. Chem*. **2015**, 3713–3720. doi:10.1002/ejoc.201500341

3. Ooyama, Y.; Uenaka, K.; Harima, Y.; Ohshita, J. *RSC Adv*. **2014**, *4*, 30225–30228. doi:10.1039/c4ra03999h

4. Enoki, T.; Ohshita, J.; Ooyama, Y. *Bull. Chem. Soc. Jpn.* **2018**, *91*, 1704–1709. doi:10.1246/bcsj.20180210

5. Guliyev, R.; Coskun, A.; Akkaya, E. U. *J. Am. Chem. Soc.* **2009**, *131*, 9007–9013. doi:10.1021/ja902584a

6. Woodford, C. R.; Frady, E. P.; Smith, R. S.; Morey, B.; Canzi, G.; Palida, S. F.; Araneda, R. C.; Kristan, Jr. W. B.; Kubiak, C. P.; Miller, E. W.; Tsien, R. Y. *J. Am. Chem. Soc*. **2015**, *137*, 1817–1824. doi:10.1021/ja510602z

7. Escudero, D. *Acc. Chem. Res*. **2016**, *49*, 1816–1824. doi:10.1021/acs.accounts.6b00299

8. Saha, M. L.; Yan, X.; Stang, P. J. *Acc. Chem. Res*. **2016**, *49*, 2527–2539. doi:10.1021/acs.accounts.6b00416

9. Mahendran, V.; Pasumpon, K.; Thimmarayaperumal, S.; Thilagar, P.; Shanmugam, S. *J. Org. Chem.* **2016**, *81*, 3597–3602. doi:10.1021/acs.joc.6b00267

10. Sandeep, A.; Praveen, V. K.; Kartha, K. K.; Karunakaran, V.; Ajayaghosh, A. *Chem. Sci.* **2016**, *7*, 4460–4467. doi:10.1039/c6sc00629a

11. Black, H. T.; Pelse, I.; Wolfe, R. M. W.; Reynolds, J. R. *Chem. Commun.* **2016**, *52*, 12877–12880. doi:10.1039/c6cc06443d

12. Ji, L.; Griesbeck, S.; Marder, T. B. *Chem. Sci.* **2017**, *8*, 846–863. doi:10.1039/c6sc04245g

13. Xu, Y.; Yu, S.; Chen, Q.; Chen, X.; Li, Y.; Yu, X.; Pu, L. *Chem. Eur. J.* **2016**, *22*, 12061–12067. doi:10.1002/chem.201601540

14. Zhou, J.; Outlaw, V. K.; Townsend, C. A.; Bragg, A. E. *Chem. Eur. J.* **2016**, *22*, 15212–15215. doi:10.1002/chem.201603284

15. Lin, S.-L.; Chan, L.-H.; Lee, R.-H.; Yen, M.-Y.; Kuo, W.-J.; Chena, C.-T.; Jeng, R.-J. *Adv. Mater.* **2008**, *20*, 3947–3952. doi:10.1002/adma.200801023

16. Park, I. S.; Komiyama, H.; Yasuda, T. *Chem. Sci.* **2017**, *8*, 953–960. doi:10.1039/c6sc03793c

17. Duan, C.; Li, J.; Han, C.; Ding, D.; Yang, H.; Wei, Y.; Xu, H. *Chem. Mater.* **2016**, *28*, 5667–5679. doi: 10.1021/acs.chemmater.6b01691

18. Huang, J.-J.; Hung, Y.-H.; Ting, P.-L.; Tsai, Y.-N.; Gao, H.-J.; Chiu, T.-L.; Lee, J.-H.; Chen, C.-L.; Chou, P.-T.; Leung, M.-K. *Org. Lett.* **2016**, *18*, 672–675. doi:10.1021/acs.orglett.5b03631

19. Zhang, Q.; Li, J.; Shizu, K.; Huang, S.; Hirata, S.; Miyazaki, H.; Adachi, C. *J. Am. Chem. Soc.* **2012**, *134*, 14706–14709. doi:10.1021/ja306538w

20. Feuillastre, S.; Pauton, M.; Gao, L.; Desmarchelier, A.; Riives,J. A.; Prim, D.; Tondelier, D.; Geffroy, B.; Muller, G.; Clavier, G.; Pieter, G. *J. Am. Chem. Soc.* **2016**, *138*, 3990–3993. doi:10.1021/jacs.6b00850

21. Hirai, H.; Nakajima, K.; Nakatsuka, S.; Shiren, K.; Ni, J.; Nomura, S.; Ikuta, T.; Hatakeyama, T. *Angew*. *Chem*. *Int*. *Ed*. **2015**, *54*, 13581–13585. doi:10.1002/anie.201506335

22. Sasabe, H.; Hayasaka, Y.; Komatsu, R.; Nakao, K.; Kido, J. *Chem*. *Eur*. *J*. **2017**, *23*, 114–119. doi:10.1002/chem.201604303

23. Yao, L.; Zhang, S.; Wang, R.; Li, W.; Shen, F.; Yang, B.; Ma, Y. *Angew*. *Chem*. *Int*. *Ed*. **2014**, *53*, 2119–2123. doi:10.1002/anie.201308486

24. Suzuki, K.; Kubo, S.; Shizu, K.; Fukushima, T.; Wakamiya, A.; Murata, Y.; Adachi, C.; Kaji, H. *Angew*. *Chem*. *Int*. *Ed*. **2015,** *54*, 15231–15235. doi:10.1002/anie.201508270

25. Mishra, A.; Fischer, M. K. R.; Bäuerle, P. *Angew. Chem. Int. Ed.* **2009**, *48*, 2474–2499. doi:10.1002/anie.200804709

26. Ooyama, Y.; Harima, Y. *Eur. J. Org. Chem.* **2009**, *18*, 2903–2934. doi:10.1002/ejoc.200900236

27. Li, X.; Zheng, Z.; Jiang, W.; Wu, W.; Wang, Z.; Tian, H. *Chem. Commun.* **2015**, *51*, 3590–3592. doi:10.1039/c4cc08539f

28. Kakiage, K.; Aoyama, Y.; Yano, T.; Oya, K.; Kyomen, T.; Hanaya, M. *Chem. Commun.* **2015**, *51*, 6315–6317. doi:10.1039/c5cc00464k

29. Wu, J.; Li, G.; Zhang, L.; Zhou, G.; Wang, Z.-S. *J. Mater. Chem. A* **2016**, *4*, 3342–3348. doi:10.1039/c6tc00178e

30. Gao, Y.; Li, X.; Hu, Y.; Fan, Y.; Yuan, J.; Robertson, N.; Hua, J.; Marder, S. R. *J. Mater. Chem. A* **2016**, *4*, 12865–12877. doi:10.1039/c6ta05588e

31. Yao, Z.; Zhang, M.; Li, R.; Yang, L.; Qiao, Y.; Wang, P. *Angew. Chem. Int. Ed*. **2015**, *54*, 5994–5998. doi:10.1002/anie.201501195

32. Brogdon, P.; Giordano, F.; Puneky, G. A.; Dass, A.; Zakeeruddin, S. M.; Nazeeruddin, M. K.; Grätzel, M.; Tschumper, G. S.; Delcamp, J. H. *Chem. Eur. J*. **2016**, *22*, 694–703. doi:10.1002/chem.201503187

33. Ooyama, Y.; Inoue, S.; Nagano, T.; Kushimoto, K.; Ohshita, J.; Imae, I.; Komaguchi, K.; Harima, Y. *Angew. Chem. Int. Ed.* **2011**, *50*, 7429–7433. doi:10.1002/anie.201102552

34. Ooyama, Y.; Sato, T.; Harima, Y.; Ohshita, J. *J*. *Mater*. *Chem*. *A* **2014**, *2*, 3293–3296. doi:10.1039/c3ta15067d

35. Sumalekshmy, S.; Gopidas, K. R. *J. Phys. Chem. B* **2004**, *108*, 3705–3712. doi:10.1021/jp022549l

36. Sumalekshmy, S.; Gopidas, K. R. *New J. Chem.* **2005**, *29*, 325–331. doi:10.1039/b409411e

37. Sumalekshmy, S.; Gopidas, K. R. *Photochem. Photobiol. Sci.* **2005**, *4*, 539–546. doi:10.1039/b503251b

38. Dias, F. B.; Pollock, S.; Hedley, G.; Pålsson, L.-O.; Monkman, A.; Perepichka, I. I.; Perepichka, I. F.; Tavasli, M.; Bryce, M. R. *J. Phys. Chem. B* **2006,** *110*, 19329–19339. doi:10.1021/jp0643653

39. Zhao, G.-J.; Chen, R.-K.; Sun, M.-T.; Liu, J.-Y.; Li, G.-Y.; Gao, Y.-L.; Han, K.-L.; Yang, X.-C.; Sun, L. *Chem. Eur. J.* **2008**, *14*, 6935–6947. doi:10.1002/chem.200701868

40. Aronica, C.; Venancio-Marques, A.; Chauvin, J.; Robert, V.; Lemercier, G. *Chemistry* **2009**, *15*, 5047–5055. doi:10.1002/chem.200802325

41. Butler, R. S.; Cohn, P.; Tenzel, P.; Abboud, K. A.; Castellano, R. K. *J. Am. Chem. Soc.* **2009**, *131*, 623–633. doi:10.1021/ja806348z

42. Ooyama, Y.; Ito, G.; Kushimoto, K.; Komaguchi, K.; Imae, I.; Harima, Y. *Org*. *Biomol*. *Chem*. **2010**, *8*, 2756–2770. doi:10.1039/c003526b

43. Enoki, T.; Matsuo, K.; Ohshita, J.; Ooyama, Y. *Phys. Chem. Chem. Phys.* **2017**, *19*, 3565–3574. doi:10.1039/c6cp08573c

44. Lippert, E. *Z. Naturforsch.* **1955**, *10*, 541–545. doi:10.1515/znb-1955-1001

45. Mataga, N.; Kaifu, Y.; Koizumi, M. *Bull. Chem. Soc. Jpn*. **1956**, *29*, 465–470. doi:10.1246/bcsj.29.465

46. Reichardt, C. *Solvents and Solvent Effects in Organic Chemistry*, VCH, Weinheim, **2003**.

47. Both the geometry optimization and energy calculation were performed by employing density functional theory (DFT), at the level of B3LYP/6-31G(d,p) on the Gaussian09 program package, Frisch, M. J.; Trucks, G. W.; Schlegel, H. B.; Scuseria, G. E.; Robb, M. A.; Cheeseman, J. R.; Scalmani, G.; Barone, V.; Mennucci, B.; Petersson, G. A.; Nakatsuji, H.; Caricato, M.; Li, X.; Hratchian, H. P.; Izmaylov, A. F.; Bloino, J.; Zheng, G.; Sonnenberg, J. L.; Hada, M.; Ehara, M.; Toyota, K.; Fukuda, R.; Hasegawa, J.; Ishida, M.; Nakajima, T.; Honda, Y.; Kitao, O.; Nakai, H.; Vreven, T.; Montgomery, J. A.; Peralta, Jr., J. E.; Ogliaro, F.; Bearpark, M.; Heyd, J. J.; Brothers, E.; Kudin, K. N.; Staroverov, V. N.; Kobayashi, R.; Normand, J.; Raghavachari, K.; Rendell, A.; Burant, J. C.; Iyengar, S. S.; Tomasi, J.; Cossi, M.; Rega, N.; Millam, J. M.; Klene, M.; Knox, J. E.; Cross, J. B.; Bakken, V.; Adamo, C.; Jaramillo, J.; Gomperts, R.; Stratmann, R. E.; Yazyev, O.; Austin, A. J.; Cammi, R.; Pomelli, C.; Ochterski, J. W.; Martin, R. L.; Morokuma, K.; Zakrzewski, V. G.; Voth, G. A.; Salvador, P.; Dannenberg, J. J.; Dapprich, S.; Daniels, A. D.; Farkas, O.; Foresman, J. B.; Ortiz, J. V.; Cioslowski, J.; Fox, D. J. Gaussian 09, Revision A.02, Gaussian, Inc., Wallingford, CT, **2009**.

48. Langhals, H.; Potrawa, T.; Nöth, H.; Linti, G. *Angew*. *Chem*. *Int*. *Ed*. **1989**, *28*, 478–480. doi:10.1002/anie.198904781

49. Yeh, H.-C.; Wu, W.-C.; Wen, Y.-S.; Dai, D.-C.; Wang, J.-K.; Chen, C.-T. *J. Org. Chem*. **2004**, *69*, 6455–6462. doi:10.1021/jo049512c

50. Ooyama, Y.; Okamoto, T.; Yamaguchi, T.; Suzuki, T.; Hayashi, A.; Yoshida, K. *Chem. Eur. J*. **2006**, *12*, 7827–7838. doi:10.1002/chem.200600094

51. Ooyama, Y.; Hagiwara, Y.; Oda, Y.; Fukuoka, H.; Ohshita, J. *RSC Adv*. **2014**, *4*, 1163–1167. doi: 10.1039/c3ra45785k